

MACH 7 TESTS OF THE LANGLEY AIRFRAME-INTEGRATED SCRAMJET

H. L. Beach, Jr.*, E. A. Mackley**, and R. W. Guy†
NASA Langley Research Center
Hampton, Virginia

Abstract

Very promising engine test results at simulated Mach 7 conditions are presented for an airframe-integrated supersonic combustion ramjet concept. Tests were conducted at the NASA Langley Research Center and at the General Applied Science Laboratories, Inc. over a simulated flight dynamic pressure range of 19 to 48 KN/m². Combustion problems that arose during early tests of the subscale (20 cm high) model were addressed by geometric changes that locally raised temperatures and pressures to enhance ignition and flameholding. Subsequent tests utilized mono-silane (SiH₄) as an ignitor and staged injection for flameholding. In this mode, performance of 90 percent of the target theoretical value has been achieved at equivalence ratios up to stoichiometric.

Nomenclature

A	geometric cowl area
$C_{\Delta F}$	$\frac{\Delta F}{q_{\infty} A_c}$, force coefficient based on force balance ΔF
H	inlet height
P	static pressure
P_1	static pressure at facility nozzle exit
q_{∞}	airstream dynamic pressure
X	distance from engine sidewall leading edge
Y	distance from engine top surface
ΔF	difference in measured force with and without fuel injection
ϕ_{injected}	equivalence ratio of injected fuel
ϕ_{reacted}	reacted equivalence ratio, $\phi_{\text{injected}} \times \eta_c$
η_c	combustion efficiency

Introduction

Background

The hypersonic propulsion research program at the NASA Langley Research Center has concentrated on the development of technology for hydrogen-fueled supersonic combustion ramjets (scramjets) since about 1964. The airframe-integrated concept providing the research focus for the present program^{1,2} is shown in figure 1. In this concept, the underside of the vehicle is an integral part of the propulsion system. The vehicle forebody provides aerodynamic precompression of the flow entering the

inlet, and the aft portion of the underside of the vehicle is used as a nozzle expansion surface. The scramjet engine captures and utilizes the precompressed airflow between the shock wave and the forebody. A group of modular engines results when this entering airflow is divided laterally into even increments. Even for a relatively large flight vehicle, one module of the group, as illustrated in the center of figure 1, then would be of a scale which could be tested in a ground facility of a feasible size.

The inlet of the rectangular scramjet engine module compresses the flow laterally by the use of wedge surfaces on swept sidewalls. The swept sidewalls and aft placement of the cowl on the underside of the engine allow for efficient spillage and good inlet starting characteristics with fixed geometry. The compression of the air in the inlet is completed by the three swept, wedge-shaped struts which are also utilized to obtain good spatial distribution of the fuel. The cross-section view of the struts in figure 1 shows that fuel is injected from the struts downstream of their maximum cross section and is injected either perpendicular to the local flow or parallel to the local flow. Since the fuel/air mixing is more rapid when the fuel is injected perpendicular to the flow than when injected parallel, the split between perpendicular and parallel fuel injection is used to control the rate of fuel/air mixing (and therefore the rate of heat release) as a function of flight Mach number. At high flight Mach number, mostly perpendicular injection and at low Mach number mostly parallel injection would be used. The control of heat release is required to efficiently operate over a flight Mach number range with a given diverging combustor geometry.

Research is currently being performed on the inlet, combustor and nozzle components of the scramjet engine module, computational fluid mechanics for internal flows, structures, and flow diagnostics.³ Based on the results of this research, two relatively small scale scramjet engine models have been designed and built. Preliminary tests have been conducted at simulated flight Mach numbers of 4 and 7,⁴ and further testing is currently underway in two different facilities. The objectives of these tests are to conduct research on the basic airframe-integrated scramjet concept, to identify performance potential, to identify problems to be addressed in other facets of the research program, and to identify changes that might be desirable in a second-generation design. It is anticipated that two or three generations (iterations) in the design will be required before final concept definition.

The purpose of this paper is to present the results and experience in the scramjet engine tests to date at conditions simulating flight Mach number 7. Preliminary (Phase I) tests at Langley were conducted in the electric arc-heated Scramjet Test Facility (STF) at a tunnel Mach number of 6.0, a stream total temperature of about 2200°K and a stream total pressure of about 30 atmospheres. This simulates a flight dynamic pressure (q_{∞}) of

* Assistant Head, Hypersonic Propulsion Branch, High-Speed Aerodynamics Division; Member AIAA

**Aerospace Engineer, Hypersonic Propulsion Branch, High-Speed Aerodynamics Division; Member AIAA

† Aerospace Engineer, Hypersonic Propulsion Branch, High-Speed Aerodynamics Division

about 0.2 atmospheres. Phase II Mach 7 tests at a flight dynamic pressure of about 0.5 atmospheres (design q_{∞}) are still in progress at the General Applied Science Laboratories, Inc. (GASL). For these tests, a combustion-heated, oxygen-replenished $M = 6$ flow at a total temperature of about 2200°K and a total pressure of about 73 atmospheres was used as the nominal test condition.

Test Philosophy

Wind tunnel facilities used to test scramjet engine models must duplicate, as far as possible, the flow under the flight vehicle forebody; this includes the flight total enthalpy (temperature) and the total pressure and Mach number ahead of the scramjet module. For flight Mach 7 simulation, the test gas is heated to temperatures of about 2200°K and expands through a nozzle to a post-bow shock simulated Mach number 6. This $M = 6$ test stream then flows into and around the scramjet engine model mounted in a test cabin. (See fig. 2.) The vehicle forebody boundary layer entering the scramjet in flight is simulated by the tunnel nozzle boundary layer on the top wall being ingested at the top of the scramjet engine model. The nozzle expansion at the aft end of the vehicle is not simulated in tunnel tests; the expansion area required is quite large, and a significantly larger facility than those presently available will be required to make such tests. Fortunately, the nozzle expansion can be treated separately both experimentally and analytically. (See ref. 5.)

Other considerations which must be made in extrapolating wind tunnel results to flight include engine mass flow adjustments due to boundary layer differences, heat transfer to the tunnel wall or vehicle forebody (and resulting wall temperature differences), external engine drag differences, and installation drag differences. It is obvious that the comparison of the wind tunnel results to flight depends critically on the detailed design of the vehicle, and the design is driven by the mission or application under consideration. Because of the ambiguities inherent in simulating an integrated engine/vehicle system, the focus in these engine tests has been on the module performance itself rather than a postulated engine/vehicle system. Theoretical predictions of acceptable performance against which the data are compared are therefore based on analysis of a single module, and usually focus on internal performance.

Apparatus and Procedure

Test Facilities

The Mach 7 facilities used for the scramjet engine tests are shown in the photographs of figures 3 and 4. The general arrangement of facility and scramjet engine model is as discussed previously and shown in figure 2. The Langley Scramjet Test Facility,⁶ is an electric arc-heated facility which utilizes two 10 megawatt d.c. power supplies connected in series. The power available limits the tunnel mass flows for the 2200°K total temperature condition, and therefore also limits the total pressure for a given size nozzle (exit 30.5 cm high by 27.2 cm wide). For the Phase I tests, the total pressure was limited to about 30 atmospheres, but this limit is currently being raised by about 30 percent by increasing the power available to the arc.

The tunnel Mach number of 6.08 and the tunnel stream total pressure of 30 atmospheres simulate the Mach number and stream total pressure under the vehicle forebody and ahead of the engine in Mach 7 flight at a flight dynamic pressure (q_{∞}) of about 0.2 atmospheres (35,150 m altitude). Similarly, at GASL, the tunnel Mach number is 6.04 (tunnel exit 27.2 cm by 27.2 cm) at the same total temperature as STF, but with a higher total pressure capability (73 atm) which allows simulation of flight dynamic pressures of about 0.5 atm (29,000 m altitude). The air is heated by the combustion of hydrogen with oxygen replenishment. The higher total pressure of the GASL facility allows testing at the design flight dynamic pressure of 0.5 atm as well as the determination, in an overall sense, of the effect of total pressure (altitude) on engine performance.

Model

The scramjet engine model used for the tests reported here is one of two which are described in reference 4. Briefly, the model is of rectangular cross section, has a frontal capture area 20.32 cm high by 16.26 cm wide, and is 151.1 cm long. (See figs. 5 and 6.) The model is constructed of copper with water cooling of the leading edges and the sidewalls near the inlet minimum area. Fuel is injected from each strut through circular fuel injector orifices as shown schematically in figure 7. For the Phase I tests, ignition/flameholding aids, involving internal geometry changes such as the aft ends of the struts, air injection tubes, and combustor sidewall insert blocks were utilized and will be discussed in a later section.

For the Phase II tests at GASL, two strut geometries were used which differed somewhat in cross section downstream of the point of fuel injection. The original strut configuration used in Phase I tests was also tested at GASL. The revised struts were contoured in cross section to reduce the expansion of the flow passages downstream of fuel injection. Also, the engine was again tested with and without the combustor sidewall insert blocks.

The scramjet engine model is heavily instrumented with 100 pressure taps, 100 thermocouples, and 50 Gardon-type heat flux gauges. For both test phases, the thrust-drag force was measured by a one-component balance; internal and external static pressures were measured by a comprehensive data system (for Phase II tests⁷); and the hydrogen fuel, gas flow rates and other pertinent parameters were measured as functions of time. The prime indicator of performance for these tests was the change in force balance measurement between fuel on and fuel off; other measurements were used mostly for diagnostic information.

Test Procedures

In the Langley STF, the test cabin and connecting duct were opened to a 20.5 m vacuum sphere; the arc-heated tunnel flow was established in the Mach 6.08 nozzle; and the scramjet engine model was inserted into the stream from the top at zero degrees angle of attack. The top surface of the model could be aligned with the top surface of the tunnel or placed one inch into the flow. During the first part of the test, the zero fuel drag level was established, and then ambient temperature

hydrogen was injected from the three engine struts. The fuel equivalence ratio was preprogrammed and automatically controlled with generally two levels (other than zero) being used each for 4 or 5 seconds.

At GASL, the test procedure was basically the same except that the scramjet model was fixed in position in the tunnel stream. The zero-fuel drag level was established in the first part of the test; then the fuel was introduced and the level changed during the test with about 2 or 3 seconds of time at each level. The fuel was shut off, and for some runs the zero-fuel level was reestablished. Test times at GASL were shorter than at STF because of the much higher heat transfer rates and potentially greater risk of model damage. When silane (SiH_4 , discussed in a later section) was used as an ignitor fuel, the silane flow rate was established, and when desired, the fuel supply was switched to hydrogen. Because of the piping and valve arrangement, the transition to hydrogen required about one second. Silane was also used as a pilot fuel; that is, it was introduced from selected fuel injectors continuously while pure hydrogen was introduced from the remaining injectors.

Phase I Results

The first tests of the airframe-integrated scramjet were conducted in the Langley Mach 7 STF using hydrogen fuel.⁴ The experimental program consisted of 111 tests and a total test time of 30 minutes. The Phase I tests were exploratory in nature since no previous engine test experience existed which was directly applicable to the airframe-integrated scramjet. The test program covered an engine operating range in which fuel equivalence ratio was varied from zero to values in excess of one. The goal was to identify problems with the scramjet concept within this range and to assess the performance potential of the engine.

Baseline Data

Pressure distributions in the scramjet engine inlet with no fuel injection are compared with inlet component data⁸ in figure 8. Agreement between the two sets of data is excellent at locations on the sidewall near the engine mid-height line and near the cowl. Peak pressures at the engine minimum cross-sectional flow area are not available for comparison with the inlet component data because of differences in pressure orifice locations in this region. The excellent agreement between the pressure distributions implies that inlet performance (i.e., mass capture, total pressure recovery, effective contraction ratio, throat Mach number, etc.) measured in the inlet component tests can be assumed valid for the engine tests.

Because many of the changes made during the Phase I tests involved geometry modifications which affected the zero-fuel drag of the engine, a performance parameter based on drag reduction (ΔF) was used as the figure of merit. ΔF is defined in figure 9 as the difference in the scramjet axial force with and without fuel injection. This assumes that the airflow entering the engine and the external drag are unchanged when fuel is injected in the engine. As shown in figure 9, even though the engine thrust depends on the change in internal force when fuel is added, it is important to keep the

internal drag low, as well as the external drag. A summary of the experimental scramjet performance obtained in the Phase I tests is shown in figure 10 where the scramjet axial force coefficient (based on ΔF normalized by cowl area and dynamic pressure) is plotted against the injected fuel equivalence ratio. Each set of performance data will be discussed in detail later in the paper. The theory shown in figure 10 is from a one-dimensional analysis with the assumption of all perpendicular fuel injection and the corresponding distribution of fuel-air mixing.⁹ Mixing-controlled reaction is assumed with 100% combustion efficiency; thus, the theory curve represents a goal against which the data can be compared.

Results Obtained with the Original Scramjet Geometry

The lowest-performance curve in figure 10 is for the original engine geometry. It is apparent from heating rate and pressure measurements that the poor performance was caused by negligible combustion. The pressure distributions of figure 11 show that even at an equivalence ratio of 0.92, only minor increases in pressure were measured relative to the zero fuel base. At ϕ_{injected} of about 1.54, large pressure rise in the cowl region occurred; this indicated a local condition near thermal choking with inlet-combustor interaction, i.e., with pressure increase upstream of the fuel injection location.

Factors which contributed to the poor combustion were the small geometric scale of the engine, low combustor entrance pressure (simulating 35,150 m altitude), rapid flow expansion just downstream of fuel injection (fig. 5), and low fuel and engine wall temperatures in the heat-sink engine. An attempt was made to improve combustion by local increases in temperature and pressure induced by geometric changes in the combustor. Although not suitable for flight engines, these changes permitted the test program to proceed so that other potential problem areas could be explored.

Effect of Modified Center Strut and Gas Injection Tubes

The first geometric changes are illustrated in figure 12. Center strut aft end modifications were added to locally decrease strut flow expansions; also, nitrogen injection from tubes downstream of the sidewall breakline was added to give an effective area change on the sidewall. The gas injection rate was approximately 7.5% of the airflow of the engine. With the smaller of the aft end modifications installed and the engine positioned to capture the facility top surface boundary layer, combustion did occur in the engine. Significant drag reduction was achieved at an equivalence ratio of about 0.4; however, with only a slight additional increase in fuel injection rate, a complete engine unstart occurred. The unstart was believed to originate in the cowl region where again large pressure rises indicated local thermal choking. Because several earlier tests with the engine at 5 degrees angle of attack suggested that thinning the engine top-surface boundary layer would increase the range of stable operating conditions, the engine was lowered 2.5 cm into the flow. Very little of the facility boundary layer was ingested as a result (boundary layer displacement thickness was about 1.5 cm). With the aid of these changes,

engine operation at an equivalence ratio in excess of 0.5 was quite stable with significant drag reduction. At an equivalence ratio of one, drag was further reduced, but an unstart occurred after about 2 seconds. In this case, the unstart appeared to be caused by the wall temperatures changing with time and inducing additional burning.

Results from tests with the indicated geometry changes and the engine lowered into the flow are shown in figure 10. Note that very little drag reduction occurred below an equivalence ratio of 0.4, for the smaller aft-end modification, and the overall performance was poor relative to the theory. However, performance was much improved over the original geometry. Both movies and pressure distribution showed that inlet-combustor interaction occurred in the cowl region well below the ϕ_{injected} values that caused an unstart. Even with the interaction, performance gains were evident until unstart occurred.

With the larger strut modification, performance was improved (relative to those with the smaller aft-end modification) over the entire equivalence ratio range. As before, local inlet-combustor interaction occurred in the cowl region, but additional fuel injection continued to produce drag reduction until unstart occurred at an equivalence ratio of one.

Pressure and heating rate distributions obtained with the gas injection tubes and larger center strut modification installed are shown in figures 13 and 14. At an injected equivalence ratio of 0.5, significant pressure and heat transfer rate increases were measured relative to the zero fuel case near the engine mid-height line. Heating rate increases were evident only downstream of the gas injection tubes while pressure increases fed upstream to the sidewall breakline. The location of the increase in heating rate may be representative of the ignition location. With $\phi_{\text{injected}} = 0.5$, pressures and heating rates also increased relative to the zero fuel case near the cowl; however, the increases extended upstream of the fuel injection location, showing local inlet-combustor interaction. Pressure rise just upstream of the gas injection tube location was large with the possibility of local thermal choking.

With $\phi_{\text{injected}} = 1.04$, pressures and heating rates throughout the engine were greatly increased. At the engine mid-height line, pressure and heating rate increases began at the fuel injection location, i.e., there was no evidence of inlet-combustor interaction at that point. Along the sidewall near the cowl, however, pressure increases were exceptionally high with a high probability that thermal choking was occurring. Both heating rates and pressures indicated a large inlet-combustor interaction near the cowl. It was this condition that caused a complete engine unstart after about 2 seconds.

The very large rises in pressure and heating near the gas injection tubes suggest a lag in combustion until the flow reaches this location; then a large amount of fuel is apparently burned. The desired situation is a mixing-controlled heat release designed to match the area expansion of the engine. The emphasis should therefore be on a requirement that combustion occur as the fuel becomes mixed with the air.

Effect of Ignitor Rods, Combustor Inserts, and Combined Perpendicular and Parallel Fuel Injection

In an effort to achieve ignition immediately downstream of fuel injection, zirconium-oxide rods were added to center strut modification 1 as shown in figure 15. Simultaneously, the combustor gas injection tubes were replaced with combustor side-wall inserts which created a constant area section for a distance of 15.2 cm downstream of the side-wall breakline. New side fuel injection struts were installed from which fuel could be injected both perpendicular and parallel to the airflow. These struts also limited flow expansion in the passages downstream of fuel injection to a maximum of 2 degrees. On some tests, loops of platinum wire were also added to the bases of all three struts to act as combustion catalysts.

Good combustion performance occurred with this configuration, and movies confirmed burning at the ignitor rods. Test results are shown in figure 10 by the shaded symbols. Fuel injection was evenly split perpendicular and parallel to the airflow. Zero fuel drag was significantly increased relative to the other geometries; however, performance based on ΔF was better than that obtained with the other geometries discussed here. The major improvement occurred at the higher values of equivalence ratio, and at a ϕ_{injected} of 1.0, the measured thrust performance was approximately 80 percent of the theoretical value. These results show that proper attention to ignition at the point of injection and a possible benefit from parallel injection can lead to much-improved performance.

Combustion Efficiency and Inlet-Combustor Interaction

Combustion efficiency was estimated for all but the shaded symbols in figure 10, using the measured heating rates and a correlation by Orth, et. al.¹⁰ In addition, during the tests using gas injection tubes and center strut modification 2, efficiency estimates were obtained using band-integration intensities of the infrared spectra from the water vapor in the scramjet exhaust gases.¹¹ The combustion efficiency results are shown in figure 16 as a function of overall equivalence ratio. For the original geometry, the results confirm that combustion was poor. For the case with gas injection tubes and small center strut modification, there is a peak at an injected fuel equivalence ratio of 0.7 and decline above and below this value. Efficiencies derived from data obtained using the gas injection tubes and the large center strut modification exhibit a continuous decline with increasing fuel equivalence ratio.

An "overall" efficiency, defined as the theoretical ϕ required to produce the measured ΔF divided by the measured ϕ_{injected} , is included on the figure for reference (dashed lines). The trend of both combustion efficiency and overall efficiency is generally similar except for the large strut modification case where the overall efficiency curve tends to peak at $\phi_{\text{injected}} = 0.5$. It should be noted that all of the overall efficiency curves fall below the values derived from heat transfer data, and therefore overall efficiency should be a conservative estimate of combustion efficiency.

Inlet-combustor interaction occurred at some value of ϕ_{injected} for all configurations. The

onset of this phenomenon is characterized in figure 17 for data obtained with gas injection tubes and center strut modifications 1 and 2. Static pressures near the engine top surface and near the cowl just upstream and opposite the fuel injectors are shown as functions of reacted equivalence ratio, defined as $\phi_{\text{reacted}} = \phi_{\text{injected}} \times \eta_c$. Looking at pressure levels in a region along the struts indicates that top-surface pressures were generally unaffected by combustion for the Phase I configurations shown. For the region near the cowl, the surface pressures were quite sensitive to the amount of fuel burned, so that there was an interaction of the combustion on the inlet flow. This interaction began at ϕ_{reacted} levels of approximately 0.3 to 0.4, and inlet unstart occurred at ϕ_{reacted} levels of about 0.5.

For the case with ignitor rods, sidewall inserts, and parallel injection, ϕ_{reacted} was not determined. However, it is clear from figure 10 that ϕ_{reacted} based on overall efficiency is 0.7 for an injected equivalence ratio 1.0; therefore the configuration differences for this case appear to be quite important.

The collective data in figure 10 show that significant performance potential does exist with the scramjet concept if effective means to insure reasonably high combustion are provided. The sensitivities to inlet-combustion interaction and unstart found in the Phase I tests were quite restrictive, however, and how much these phenomena were impacted by the geometry modifications is not known. Since these modifications were made for the most part to raise the local pressure and temperature, improved burning with a "clean" engine is essential to the determination of whether the ϕ_{reacted} limits are inherent to the concept or geometry-modification dependent.

Phase II Results

Based on results of the Phase I tests and a series of calculations on the effect of pressure on the chemistry in a scramjet combustor, a decision was made to test the engine at GASL to take advantage of its higher pressure capability. In an effort to directly determine the facility pressure effect, the geometric modifications introduced in the Phase I tests were removed, and the engine was installed at GASL in a configuration close to the original one. Potentially important changes were incorporated, however. Fuel injection from the top and bottom fuel injection orifices was eliminated to reduce potential for local thermal choking in sensitive regions of the engine, as indicated in figure 7. Also, the top surface boundary layer problem was by-passed by dropping the engine 1.9 cm into the flow, and the fuel injection orifices were moved further downstream of the steps as indicated by reference 12.

The first tests in the Phase I program were at low pressure to see if the earlier results could be duplicated. Since no ignition or flameholding aids were included, this was essentially an examination of the effect of using a combustion-heated (water-vitiated) test gas as opposed to an arc-heated test gas. Although the vitiated test gas has a different molecular weight and effective specific heat ratio than those of air, the results at low pressure were essentially the same as those at the arc-heated

facility, and indicated no significant test gas effect (free radical or otherwise) on combustion. When the pressure level of the heater was increased up to the design flight dynamic pressure simulation value of 47.9 KPa, there was no dramatic change in the burning characteristics, and relatively little combustion was again achieved. This result indicated that pressure alone would not solve the combustion problems for the clean engine configuration.

At this point in the test program, two very important decisions were made regarding ignition and flameholding. Based on literature information on hydrogen compatibility and some preliminary bench-type tests, mono-silane (SiH_4) was introduced as a positive ignition source. Based on experience in the Hypersonic Research Engine project¹³ and other engine test programs, staged injection was added to locally increase the fluid dynamic scale to enhance flameholding. The impact of these two changes was large, and is discussed in subsequent sections.

Effect of Silane

Mono-silane, also called silane or silicon tetrahydride (SiH_4), is a colorless gas. Since silicon is a member of the Group IV elements appearing directly below carbon on the periodic table, the silane molecule is analogous to methane. Like carbon hydrides, silicon hydrides of the form $\text{Si}_n\text{H}_{2n+2}$ may occur; however, only those up to $n = 3$ or 4 have been produced.

In the past, silanes in organo-metallic compounds have been investigated as potential fuels for rockets. To our knowledge, pure silanes have never been used either as primary fuel, or ignition/pilot aids for any rocket or airbreathing engine concept. However, mono-silane (SiH_4) appears very attractive as a combustion aid in ground tests of hydrogen-fueled supersonic combustion ramjets. At ambient temperatures, silane is a gas that is readily compatible with existing hydrogen fuel systems. It auto-ignites at temperatures well below ambient over a wide range of equivalence ratios. For example, at concentrations as low as 2 percent by volume, silane will react spontaneously in an oxygen atmosphere at ambient temperature to produce SiO_2 and H_2O . The heat release in this reaction (heat of combustion) is 27.5 kJ/g of silane; this corresponds to 120 kJ/g for hydrogen. The heat release per unit oxidizer is, however, about the same as hydrogen, and resulting flame temperatures are also comparable.

Silane can be purchased from gas suppliers in any mixture ratio with hydrogen. The bench tests (at GASL) indicated that a 20/80 percent by volume silane/hydrogen mixture would readily burn at room temperature; this mixture ratio was therefore used in the Mach 7 engine tests. Further information on the use of silane as an ignition-pilot fuel can be found in reference 14.

Silane-hydrogen mixtures were introduced into the engine through the usual fuel injection orifices. The hope was that a flame could be established using silane, and that a transition from silane-hydrogen mixtures to pure hydrogen could be accomplished without losing the flame. A typical result is shown in the static pressure distribution of figure 18. For this case, the overall equivalence ratio was 0.636, and no fuel was injected

into the side passages between the side struts and the sidewalls. The data are for no fuel, for hydrogen with silane, and for hydrogen only. The operational sequence involved the introduction of the 20/80 percent silane/hydrogen mixture from all perpendicular and parallel injector holes for approximately one second, and then the replacement of this mixture with hydrogen alone. Of the indicated fuel equivalence ratio for silane and hydrogen, approximately 0.3 was from the silane and 0.336 from hydrogen. It is apparent that substantial burning did occur with silane piloting, but the fire essentially went out when the silane flow was terminated. Note that even when the fuel was burning, the effect on the sidewall pressures did not appear until some distance downstream of injection. The apparent "valley" in the pressure distribution is common for this engine concept, and is discussed by Northam, et al.¹⁵ The extent of the valley may be important to flameholding, and here it appears that the flame will not hold with this configuration at this scale even with a positive ignition source and a considerable initial combustion disturbance.

Effect of Staged Injection

In order to improve flameholding characteristics, two changes were made to the configuration. First, because of improvements in combustion experienced in the Phase I tests, the sidewall inserts were re-installed. Second, staged fuel injection was added. This change, as illustrated in figure 19, involves an increase in the size of the separated, recirculating regions in the vicinity of perpendicular fuel injectors by the addition of another set of injectors just downstream of the existing set. With staged injection, the downstream separated zone of an upstream injector interacts with the upstream separated zone of the downstream injector to produce a large disturbed region more appropriate for flameholding. Due to fuel manifold limitations in the struts, the second stage was located approximately 1.25 cm downstream of the first stage (except in the side passage, where staging was not possible). This distance, however, was believed to be reasonable based on comparisons of stage spacing-to-boundary-layer thickness ratios in the prior test program.¹³

An indication of the effect of these changes is given by figure 20. Data for no fuel, silane and hydrogen (silane $\phi = 0.15$), and hydrogen only are again shown. In this test, the silane-hydrogen mixture was injected into the first fuel injection stages on the center strut, and into both stages on the side strut center passage. Pure hydrogen was injected from all the second stage center strut and all parallel orifices. (There was no fuel in the side passages). After establishing the flame, the silane-hydrogen mixture was replaced with pure hydrogen. In contrast to figure 18, the pressure distribution established with silane was maintained after the silane is removed; successful flameholding was therefore achieved. The performance figures for the condition with and without silane were $C_{\Delta F}$ of .514 and .394, which correspond to 70 percent and 67 percent of the theoretical values at their respective equivalence ratios. It should be noted that the amount of combustion implied by these results represents a level of ϕ_{reacted} about the same as the limit indicated by the Phase I tests for inlet unstart (ϕ_{reacted} was .48 based on the overall efficiency).

Improvement in the performance relative to theory probably requires better fuel distribution with injection in the side passages. Attempts to raise the equivalence ratio in this manner did not prove successful, however. Inlet-combustor interactions and unstarts typically occurred with equivalence ratios above those indicated in figure 20, and the constraints on fuel manifolding and controls precluded an optimization of fuel distribution to minimize the problem. Again, based on Phase I test experience with inlet-combustor interactions aggravated by the sidewall inserts, these inserts were removed. Figure 21 shows the effect of this change on the pressure distribution for two runs at equivalence ratios of 0.67. There is obviously a very large difference in the pressure level caused by the inserts; the peak pressures are higher by a factor of approximately two and remain higher for a significant distance through the combustor. There is a crossover in the pressure distributions at the $x/H = 5.2$ station, however. It is important to note that the performance level as measured by $C_{\Delta F}$ in these two runs is the same. This occurs because a significant portion of the very high-pressure region with inserts is in a constant area section with no rearward facing surface, while the area change over which the higher pressures without inserts occurs ($x/H > 5.2$) is very large. The result is that the pressures and areas compensate to keep the pressure-area integral the same. To some extent this result may be coincidental in that it is conceivable that the crossover in pressure would not occur if the inserts had a different, more efficient shape. It is true, however, that for this configuration with very blunt-based inserts the performance is the same with and without inserts; this conclusion is confirmed by integrations of the pressure and skin friction (derived from heat flux data). Because the overall performance was not affected by the removal of the inserts, the remainder of the test program was conducted without the sidewall inserts.

A number of runs were made with different fuel injection patterns, different facility pressures, and different amounts of silane in order to determine the effects of these changes on overall engine performance with silane piloting. Figure 22 illustrates the effect of fuel distribution on pressure distribution and performance. The top curve represents a case where the fuel was fairly evenly spread among the various fuel passages. In the curve labeled non-uniform, most of the fuel was injected from the side struts, and the center strut was operating very fuel lean. Combustion in the center passage was apparently delayed quite significantly, and the resulting performance figures indicate a decrease in performance for the non-uniform case of 30 percent even though the equivalence ratio is 15 percent higher.

Not only is overall fuel distribution critical to performance, but it is also critical to establish a flame in every passage where fuel is injected. Relying on flame propagation to ignite a significant part of the fuel is very ineffective since ignition will occur far downstream if at all. An illustration of this point is shown in figure 23, which compares two runs in which the overall fuel is fairly well-distributed, but one has hydrogen only in the side passages. The pressures, beginning with a larger "valley" are consistently lower for the case with no side-passage silane. The difference in performance by a factor of about

2 in C_{AF} far exceeds the relatively small (25 percent) difference in equivalence ratio.

Figure 24 shows that if the overall fuel and silane distributions are reasonably uniform, then the overall equivalence ratio, the facility stagnation pressure, and the silane equivalence ratio do not produce major effects on the character of the pressure distributions. For the 75 atm run (47.9 kPa flight dynamic pressure simulation), the overall equivalence ratio was 0.83, of which approximately 0.35 was silane; the silane/hydrogen mixture was injected from all second stage perpendicular orifices and the side strut parallel orifices. For the 47.5 atm case (31 kPa flight dynamic pressure simulation) the overall equivalence ratio indicated was 0.67 (0.05 silane), and silane was introduced through the center strut first stage, the side strut first and second stages, and the side passage. With silane from the same locations, the 34 atm case (22.6 kPa flight dynamic pressure simulation) is for an equivalence ratio of 1.0 (0.09 silane). The results show conclusively that silane-piloted flows exhibit substantial combustion over a range of pressures and equivalence ratios.

Performance Summary

The significance of the amount of combustion indicated in the previous figures from the overall engine performance standpoint is illustrated in figure 25. This is a plot of the performance parameter C_{AF} as a function of equivalence ratio for selected data from the Phase II tests. The plot shows that silane-piloted performance levels are on the order of 90 to 100 percent of those desired, and hydrogen-only performance levels are somewhat lower. These data cover a wide range of silane and hydrogen equivalence ratios, simulated flight dynamic pressures, and initial conditions. The reduced performance for hydrogen is related to the fact that most hydrogen transition runs were made with poor fuel distribution which resulted in poor performance with and without silane. The resolution of hydrogen-only performance will be accomplished through on-going tests and more extensive data analysis. At any rate, the performance levels with and even without silane are considered to be extremely encouraging for the airframe-integrated scramjet concept. No attempt has yet been made to optimize the fuel injection geometries or the engine contours, yet the performance still far exceeds that in the earlier tests. It has been shown conclusively that the airframe-integrated scramjet concept can achieve high performance at high equivalence ratio, and the "limits" observed in the Phase I tests appear to be a result of the geometric changes and fuel injector locations rather than due the basic concept itself. Both silane and staged injection appear to be important in achieving these results in that they assure stable burning at the point of injection.

The remaining tasks in the Phase II tests are to further explore the top-surface boundary layer effects and to demonstrate silane-like performance with hydrogen alone at high equivalence ratio. The implications of the experience to date leads to considerable optimism that these issues will be resolved in the very near future in subsequent tests.

Summary and Conclusion

Two phases of research engine tests of the Langley airframe-integrated scramjet concept have been performed in two facilities capable of simulating Mach 7 flight. These tests have collectively identified problems, stimulated new basic and component research, and, ultimately, demonstrated excellent performance potential.

In the Phase I tests, low facility pressures coupled with small engine scale led to ignition and flameholding problems. These problems were circumvented by actual geometric changes and effective geometric changes induced by gas injection; combustion was significantly enhanced by these techniques. The best data involved the use of ignitor rods on the fuel injection struts, a large addition to the center strut to limit strut area divergence, and sidewall insert blocks to constrain the divergence in the combustor near-field downstream of the struts. These changes caused combustion to begin near the point of injection, and gave approximately 80 percent of theoretical performance at an equivalence ratio of one. For other configurations, inlet-combustor interactions occurred for reacted equivalence ratios above about 0.4, and complete engine unstart occurred for reacted equivalence ratios greater than 0.5. The fact that the "best" configuration described above seemed to exceed these limits was an indication that good and stable performance is dependent on the establishment of the flame at the point of injection.

The Phase II tests, using essentially a "clean" engine configuration, showed that increased pressure alone would not insure the type of combustion performance required. Rather than going back to geometry changes, pyrophoric silane was added to insure ignition at the point of injection, and staged injection was added to locally increase the injection disturbance scale in order to enhance flameholding. This combination achieved 90 to 100 percent of theoretical performance over a range of equivalence ratios with silane piloting, and gives considerable optimism for comparable hydrogen-only performance in further tests.

Based on the results presented, it is clear that the performance potential of the airframe-integrated scramjet concept has been demonstrated for Mach 7. There are remaining questions to be answered, for example concerning top-wall boundary layers, and performance must still be demonstrated at low Mach numbers (around 4). However, optimism is high that through attention to identified problems and through optimization of the configuration in a second-generation design, the airframe-integrated scramjet will be a viable technology option for the country.

Acknowledgments

This paper presents results of a research endeavor involving significant contributions from many persons in the Hypersonic Propulsion Branch at NASA-Langley Research Center and at the General Applied Science Laboratories, Inc. Input and assistance from these persons are greatly appreciated.

References

1. Henry, J. R.; and Anderson, G. Y.: Design Considerations for the Airframe-Integrated Scramjet. Presented at the 1st International Symposium on Air Breathing Engines, Marseille, France, June 19-23, 1972.
2. Jones, R. A.; and Huber, P. W.: Toward Scramjet Aircraft. *Astronautics and Aeronautics*, Vol. 16, No. 2, Feb. 1978, pp. 38-48.
3. Beach, H. L.: Hypersonic Propulsion - Aeropropulsion 1979. NASA CP 2092, 1979, pp. 387-401.
4. Guy, R. W.; and Mackley, E. A.: Initial Wind Tunnel Tests at Mach 4 and 7 of a Hydrogen-Burning, Airframe-Integrated Scramjet. AIAA Paper No. 79-7045, Apr. 1979, pp. 347-358.
5. Hunt, J. L.; Talcott, N. A., Jr.; and Cubbage, J. M.: Scramjet Exhaust Simulation for Hypersonic Aircraft Nozzle Design and Aero Model Tests. AIAA Paper No. 77-82, Jan. 1977.
6. Boatright, William B.; Sabol, Alexander P.; Sebacher, Daniel I.; Pinckney, Shimer Z.; and Guy, Robert W.: Langley Facility for Tests at Mach 7 of Subscale, Hydrogen-Burning, Airframe-integratable Scramjet Models. AIAA Paper No. 76-11, Jan. 1976.
7. Trexler, C. A.: Instant Replay Data System for Combustion Tests. Presented at the 17th JANNAF Combustion Meeting, Hampton, Virginia, Sept. 22-26, 1980.
8. Trexler, C. A.; and Souders, S. W.: Design and Performance at a Local Mach Number of 6 of an Inlet for an Integrated Scramjet Concept. NASA TN D-7944, Aug. 1975.
9. Pinckney, S. Z.: Internal Performance Predictions for Langley Scramjet Engine Module. NASA TM X-74038, Jan. 1978.
10. Orth, R. C.; Billig, F. S.; and Grenleski, S. E.: Measurement Techniques for Supersonic Combustion Testing. *AIAA Progress in Astronautics and Aeronautics*, Vol. 34, Jan. 1974.
11. Reid, R. A.; and Slack, M. N.: Infrared Measurements of a Scramjet Exhaust. NASA CR-3242, Jan. 1980.
12. McClinton, C. R.: Autoignition of Hydrogen Injected Transverse to Supersonic Airstream. AIAA Paper 79-1239, June 1979.
13. Engineering Staff, AiResearch Manufacturing Company of California: Hypersonic Research Engine Project - Phase II. Aerothermodynamic Integration Model Development. NASA CR-132654, May 1975.
14. Beach, H. L.; Mackley, E. A.; and Rogers, R. C.: Use of Silane in Scramjet Research. Presented at the 17th JANNAF Combustion Meeting, Hampton, Virginia, Sept. 22-26, 1980.
15. Northam, G. B.; Trexler, C. A.; and Anderson, G. Y.: Characterization of a Swept-Strut Hydrogen Fuel Injector for Scramjet

Applications. Presented at the 15th JANNAF Combustion Meeting, Newport, Rhode Island, Sept. 11-15, 1978.

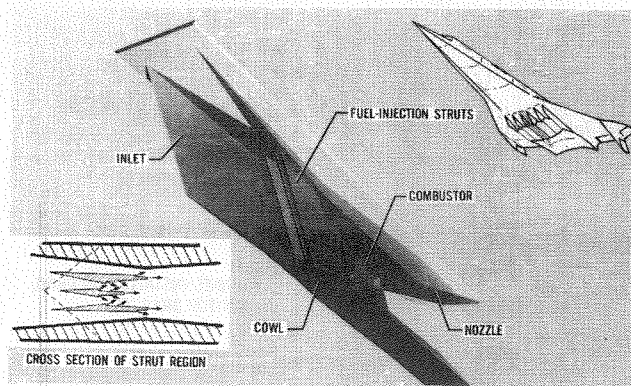


Fig. 1 Airframe-integrated supersonic combustion ramjet.

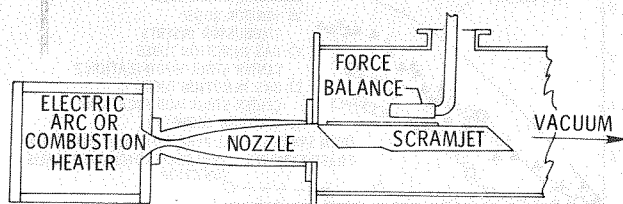


Fig. 2 Facility test schematic.

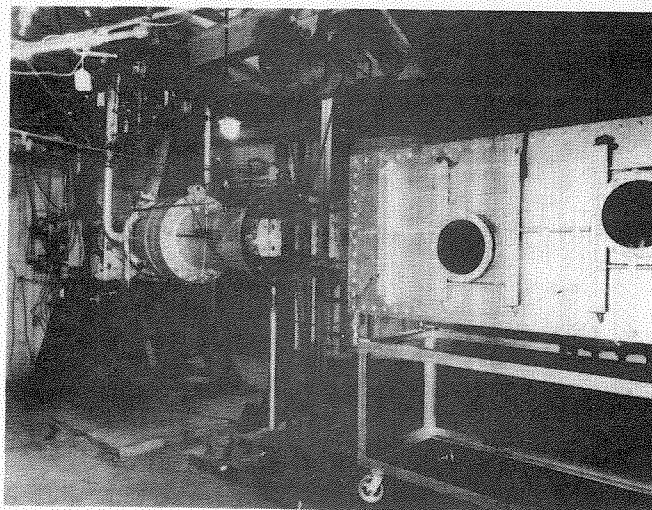


Fig. 4 General Applied Science Laboratory combustion-heated test facility.

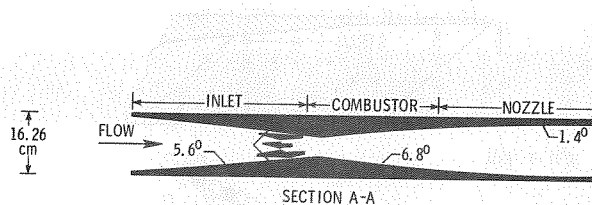
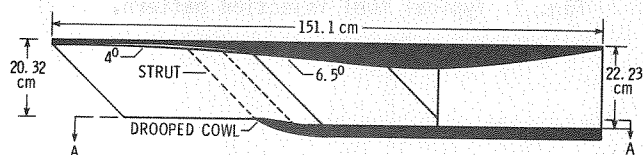


Fig. 5 Schematic of engine cross-section.

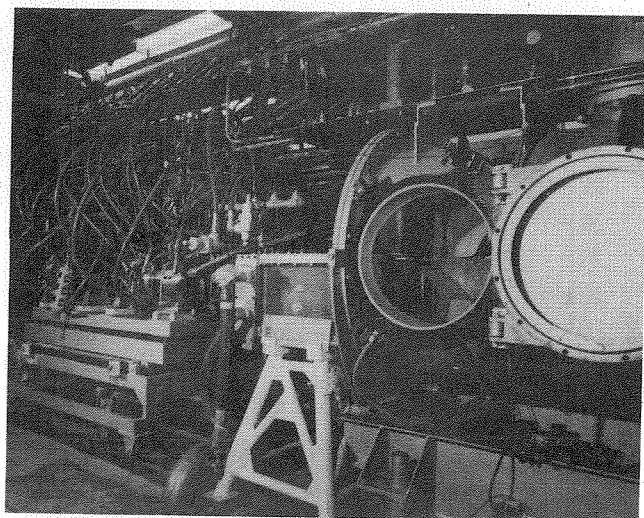


Fig. 3. Langley arc-heated scramjet test facility.

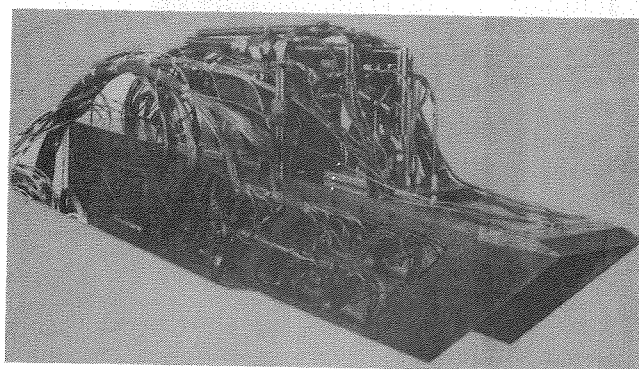


Fig. 6 Scramjet test model.

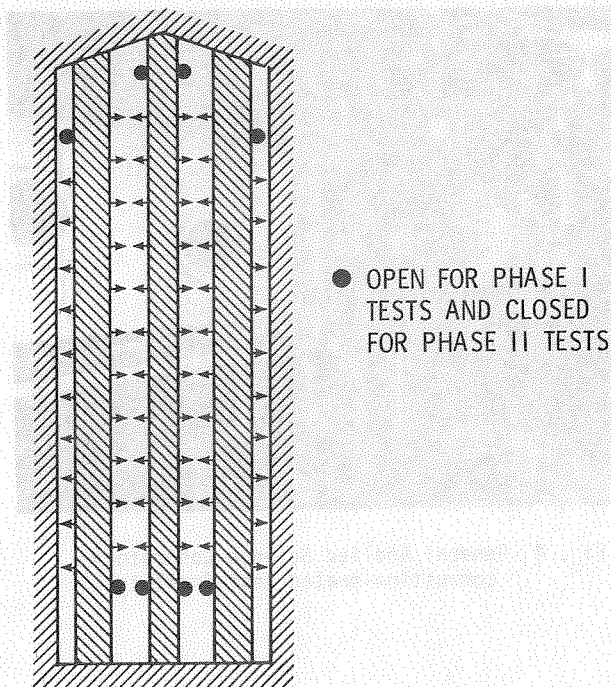


Fig. 7 Typical fuel injection pattern.

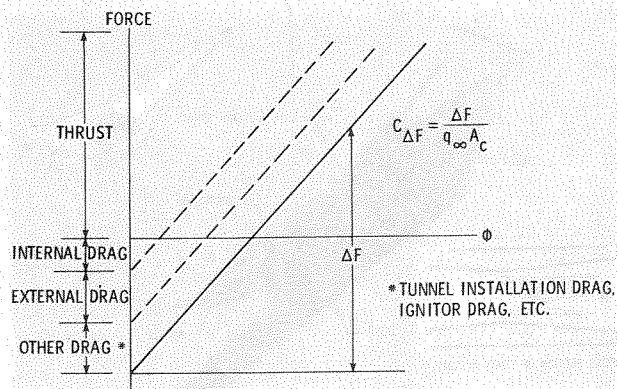


Fig. 9 Definition of performance parameter.

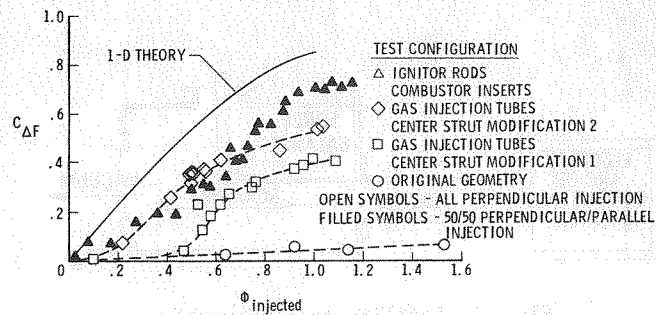


Fig. 10 Phase I performance with geometric combustion aids.

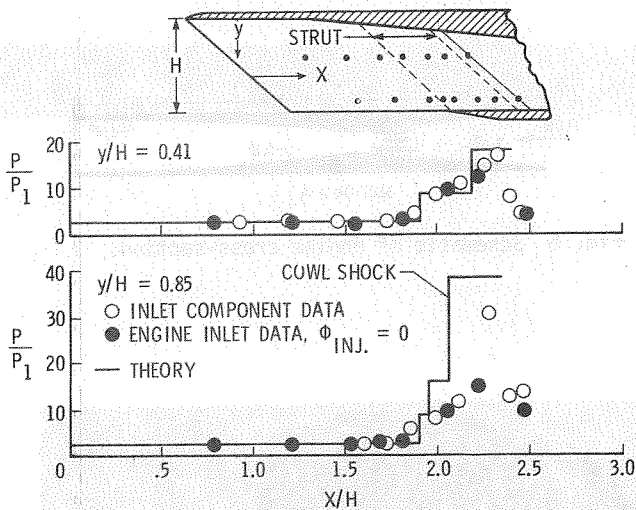


Fig. 8 Verification of inlet starting and performance.

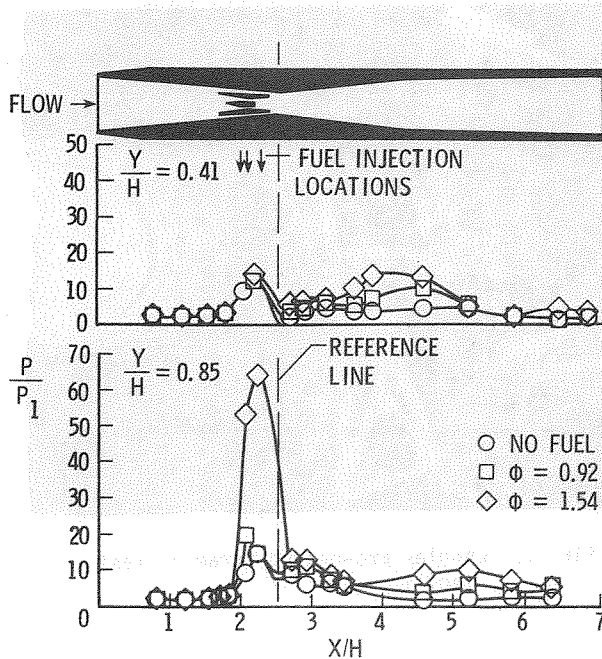


Fig. 11 Phase I pressure distributions with original geometry.

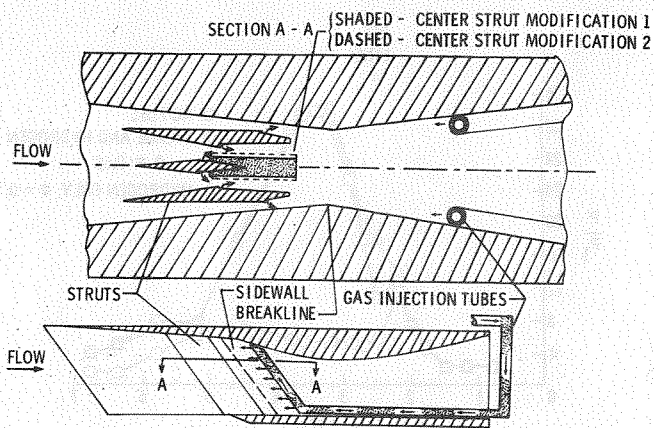


Fig. 12 Strut modifications with gas injection tubes.

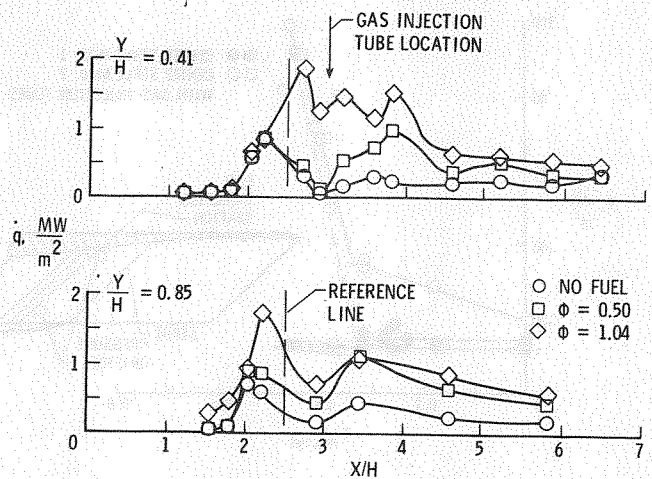


Fig. 14 Phase I heat transfer rate distributions with strut modification and gas injection tubes.

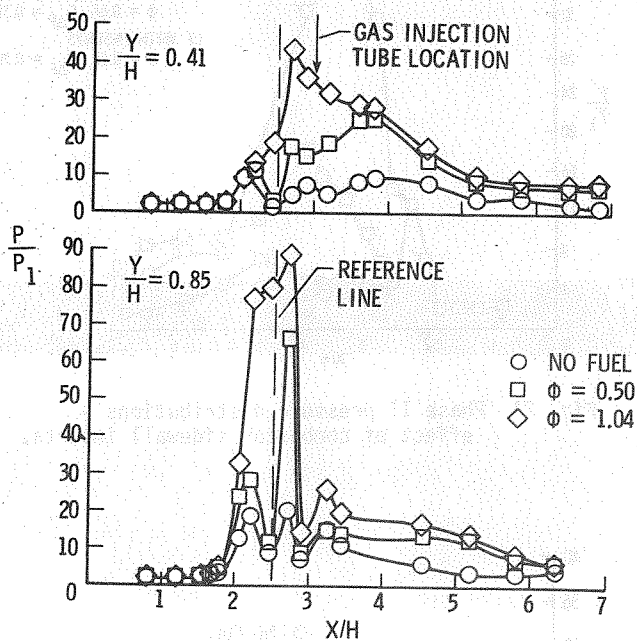


Fig. 13 Phase I pressure distributions with strut modification and gas injection tubes.

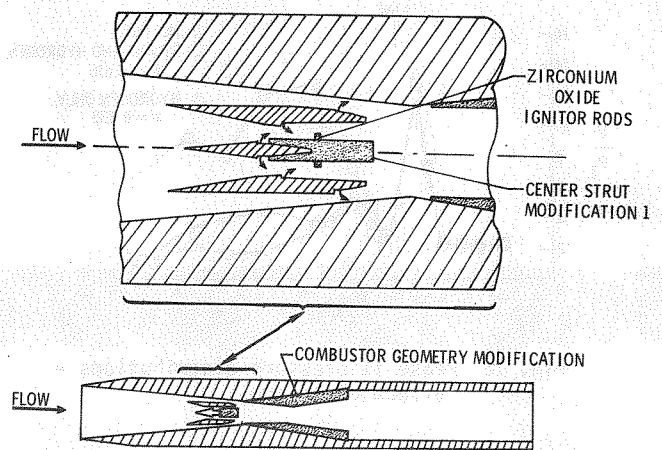


Fig. 15 Ignitor rods and combustor sidewall inserts.

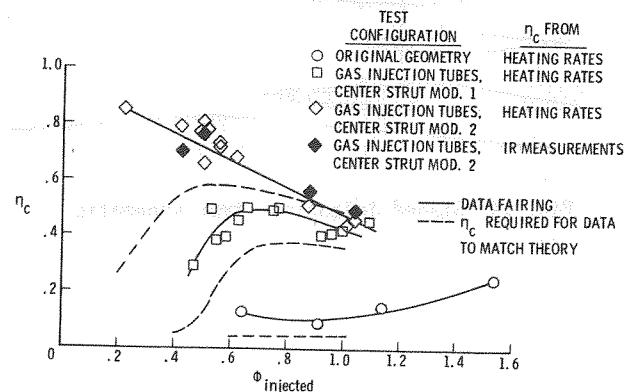


Fig. 16 Phase I combustion efficiency.

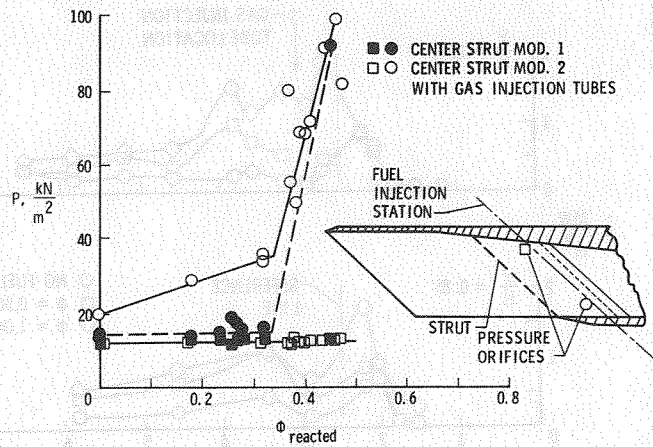


Fig. 17 Phase I inlet-combustor interaction.

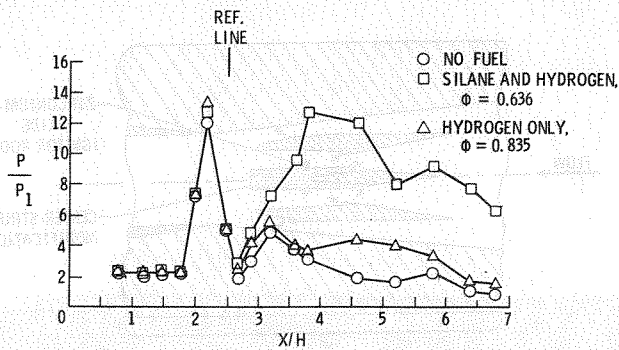


Fig. 18 Phase II pressure distributions - effect of silane.

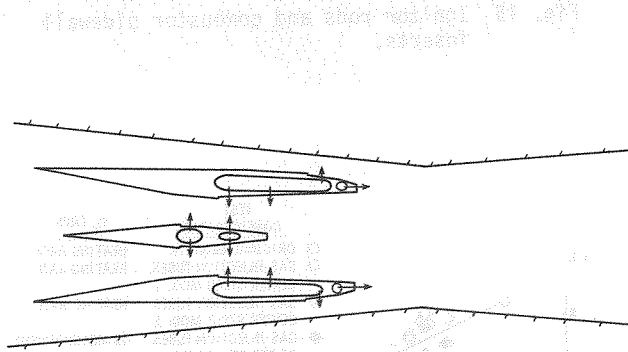


Fig. 19 Staged injection strut schematic.

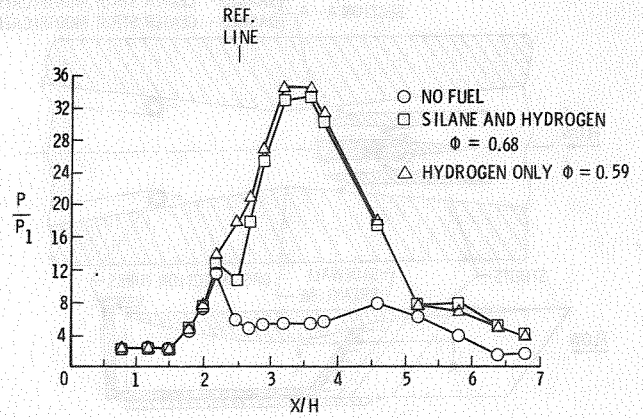


Fig. 20 Phase II pressure distributions - flameholding with silane and staged injection.

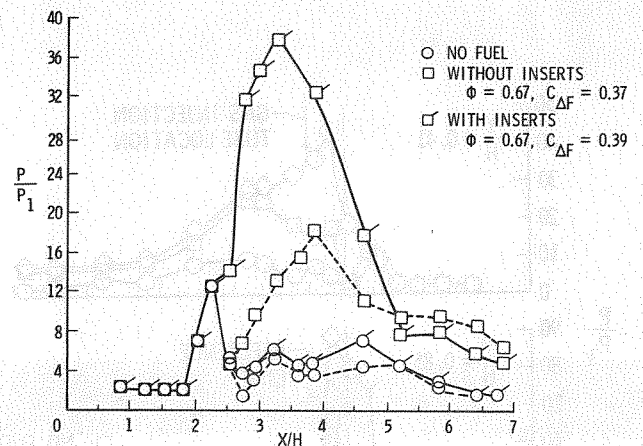


Fig. 21 Phase II pressure distributions - effect of combustor sidewall inserts.

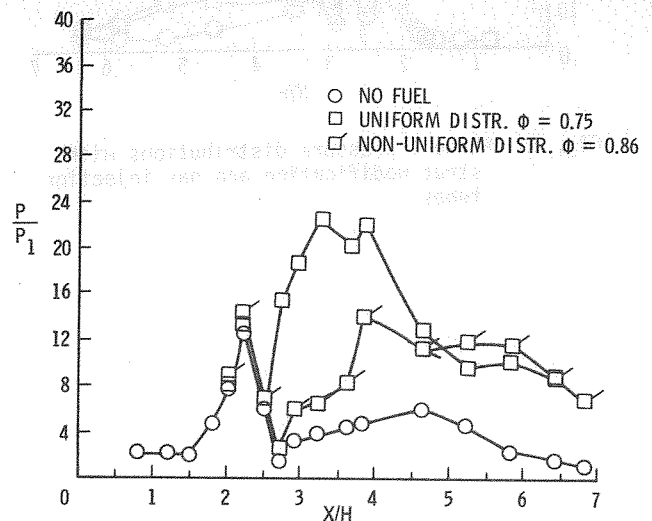


Fig. 22 Phase II pressure distributions - effect of fuel distribution.

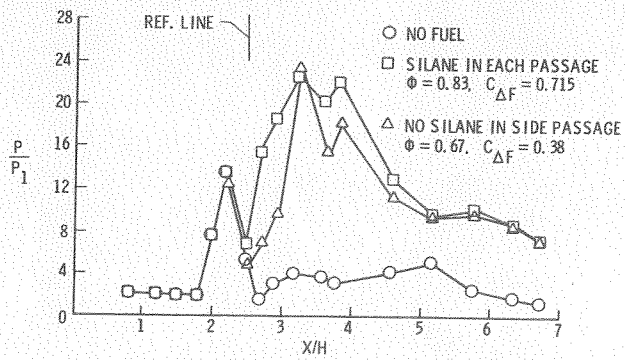


Fig. 23 Phase II pressure distributions - importance of silane distribution.

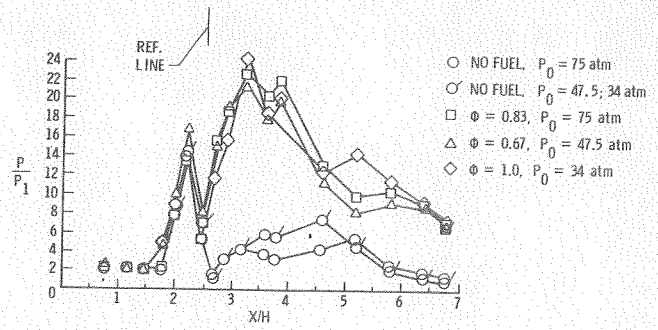


Fig. 24 Phase II pressure distributions - effect of facility stagnation pressure.

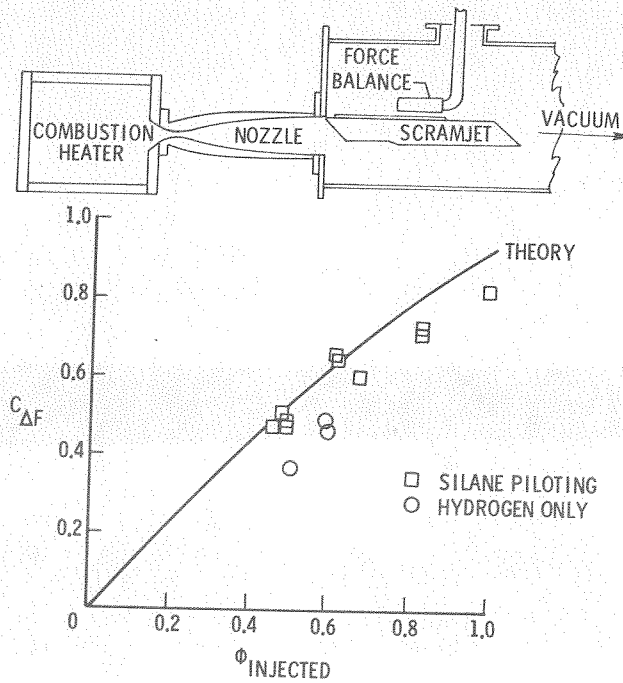


Fig. 25 Phase II performance with silane and staged injection.